Accepted Manuscript

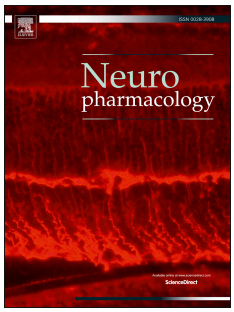

Discovery and molecular interaction studies of a highly stable, tarantula peptide modulator of acid-sensing ion channel 1

Sing Yan Er, Ben Cristofori-Armstrong, Pierre Escoubas, Lachlan D. Rash

PII: S0028-3908(17)30112-0

DOI: 10.1016/j.neuropharm.2017.03.020

Reference: NP 6638

To appear in: *Neuropharmacology*

Received Date: 25 January 2017

Revised Date: 5 March 2017

Accepted Date: 17 March 2017

Please cite this article as: Er, S.Y., Cristofori-Armstrong, B., Escoubas, P., Rash, L.D., Discovery and molecular interaction studies of a highly stable, tarantula peptide modulator of acid-sensing ion channel 1, *Neuropharmacology* (2017), doi: 10.1016/j.neuropharm.2017.03.020.

Discovery and molecular interaction studies of a highly stable, tarantula peptide modulator of acid-sensing ion channel 1

Sing Yan Er[a,1], Ben Cristofori-Armstrong[a,1], Pierre Escoubas[b], and Lachlan D. Rash[a,c,*]

[a]Institute for Molecular Bioscience, The University of Queensland, St Lucia, QLD 4072, Australia

[b]VenomeTech, 473 Route des Dolines, Villa 3, 06560 Valbonne, France

[c]School of Biomedical Sciences, The University of Queensland, St Lucia, QLD 4072, Australia

[1]Contributed equally

***Address for correspondence**

Dr Lachlan D. Rash: School of Biomedical Sciences, The University of Queensland, St Lucia, QLD 4072, Australia; Phone: +61 7 3346 2985; E-mail: l.rash@uq.edu.au.

ABSTRACT

Acute pharmacological inhibition of acid-sensing ion channel 1a (ASIC1a) is efficacious in rodent models in alleviating symptoms of neurological diseases such as stroke and multiple sclerosis. Thus, ASIC1a is a promising therapeutic target and selective ligands that modulate it are invaluable research tools and potential therapeutic leads. Spider venoms have provided an abundance of voltage-gated ion channel modulators, however, only one ASIC modulator (PcTx1) has so far been isolated from this source. Here we report the discovery, characterization, and chemical stability of a second spider venom peptide that potently modulates ASIC1a and ASIC1b, and investigate the molecular basis for its subtype selectivity. π-TRTX-Hm3a (Hm3a) is a 37-amino acid peptide isolated from Togo starburst tarantula (*Heteroscodra maculata*) venom with five amino acid substitutions compared to PcTx1, and is also three residues shorter at the C-terminus. Hm3a pH-dependently inhibited ASIC1a with an IC_{50} of 1–2 nM and potentiated ASIC1b with an EC_{50} of 46.5 nM, similar to PcTx1. Using ASIC1a to ASIC1b point mutants in rat ASIC1a revealed that Glu177 and Arg175 in the palm region opposite α-helix 5 play an important role in the Hm3a-ASIC1 interaction and contribute to the subtype-dependent effects of the peptide. Despite its high sequence similarity with PcTx1, Hm3a showed higher levels of stability over 48 hours. Overall, Hm3a represents a potent, highly stable tool for the study of ASICs and will be particularly useful when stability in biological fluids is required, for example in long term *in vitro* cell-based assays and *in vivo* experiments.

Keywords: Acid-sensing ion channel 1, Hm3a, venom, peptide, structure-activity relationship, peptide stability

1. Introduction

Over the last two decades, the growing knowledge on the molecular basis of various channelopathies and neurological disorders has fuelled an intense interest in the discovery and development of ion channel modulators as therapeutics and pharmacological tools (Bagal et al., 2013). Spiders, in particular, have proved to be a rich source of such modulators. Their venoms contain numerous biologically active peptides that potently target a variety of ion channels (Klint et al., 2012; Saez et al., 2010). As such, peptides isolated from spider venoms have been widely used to dissect the molecular mechanisms of channel function and their role in biological processes (Nebe et al., 1999; Osteen et al., 2016; Siemens et al., 2006). In this respect, the acid-sensing ion channels (ASICs) are no different with a spider venom peptide being the first, and still the most potent, selective modulator known for ASICs.

ASICs are chordate-specific members of the degenerin/epithelial sodium channel family that are widely distributed in the nervous system and many non-neuronal cells (Boscardin et al., 2016). They are primary mammalian acid sensors and as such are activated by protonation (Waldmann et al., 1997). Six ASIC subtypes are known (ASIC1a/b, ASIC2a/b, ASIC3 and ASIC4), which can assemble as functional homotrimeric (ASIC1a/b, ASIC2a and ASIC3 only) or heterotrimeric channels (Hesselager et al., 2004; Jasti et al., 2007). Each subunit consists of a large extracellular domain, two transmembrane helices, and short intracellular N- and C-termini. The combination of subunits in each channel affects the pH sensitivity, pharmacology, and kinetics of activation and desensitization (Hesselager et al., 2004). ASIC1a is the most abundant ASIC subunit in the mammalian central nervous system. Unlike other ASICs, ASIC1a is also permeable to Ca^{2+}, a property that has been associated with ASIC1a's role in acidosis-induced neuronal injury (Xiong et al., 2004; Yermolaieva et al., 2004). ASICs have been implicated with a variety of pathophysiological conditions such as inflammatory and neuropathic pain (Bohlen et al., 2011; Deval et al., 2008; Duan et al.,

2007), psychiatric illness (Coryell et al., 2009), multiple sclerosis (Vergo et al., 2011), epileptic seizure termination (Ziemann et al., 2008) and ischemic stroke (McCarthy et al., 2015; Xiong et al., 2004), hence are considered promising therapeutic targets (Wemmie et al., 2013).

Although several small molecules have been demonstrated to modulate ASIC activity, they lack subtype specificity and potency, and are limited in their usefulness as pharmacological tools. In contrast, venom peptides are often extremely potent and can have very high selectivity for neuronal targets (Klint et al., 2012). To date, six ligands targeting various ASIC subtypes have been isolated from animal venoms (Baron and Lingueglia, 2015), The prototypical and therefore most studied ASIC ligand is the spider venom peptide, PcTx1, from the spider *Psalmopoeus cambridgei* (Escoubas et al., 2000). PcTx1 inhibits homomeric ASIC1a with an IC_{50} of ~0.9 nM, and stabilizes the open state of ASIC1b. More recently it has been shown to also inhibit heteromeric ASIC1a/2b and ASIC1a/2a channels (Joeres et al., 2016; Sherwood et al., 2011). The only other inhibitory peptide ligands of ASIC1 include the mambalgins, from the Mamba snakes (*Dendroaspis* spp.), which have been shown to inhibit ASIC1a and ASIC1b containing channels with IC_{50} values between 11 and 300 nM (Baron and Lingueglia, 2015; Diochot et al., 2012).

In a functional screening of a panel of spider venoms, we observed ASIC1a inhibitory activity from the venom of the Togo starburst tarantula (*Heteroscodra maculata*). Here, we describe the isolation, recombinant expression and characterization of a second potent inhibitor of ASIC1a. The peptide named π-theraphotoxin-Hm3a (hereafter Hm3a), was pharmacologically characterized to determine its ASIC subtype-selectivity, binding site, mechanism of action and stability.

2. Materials and Methods

2.1 Venom peptide purification and characterization

Heteroscodra maculata venom was purchased from Spider Pharm (Yarnell, AZ, USA). The lyophilized venom was dissolved in water (1:10 dilution from original venom volume) and stored at –20 °C until required. A total of 50 µL of the diluted venom was fractionated using RP-HPLC on a C18 column (Phenomenex Kinetex, 250 x 4.6 mm, 100Å) using a gradient of solvent A (0.05% trifluoroacetic acid (TFA) in H_2O) and solvent B (90% acetonitrile, 0.043% TFA in H_2O) as follows: 5% solvent B for 5 min, 5–20% solvent B for 10 min, 20–50% solvent B for 30 min, 50–80% solvent for 5 min, at a flow rate of 1 mL/min. Fractions were collected by monitoring eluent absorption at 214 and 280 nm and lyophilized. The dried fractions were dissolved in water and aliquots of each fraction were assayed for activity against rASIC1a expressed in *Xenopus* oocytes. A second RP-HPLC purification was carried out on the active fraction using a C18 column (Thermo Aquasil, 50 × 2.1 mm, 190Å) and a gradient of 10–30% solvent B over 20 min at a flow rate of 0.3 ml/min. All solvents used were HPLC grade.

2.2 RP-HPLC and MALDI-TOF mass spectrometry

Both analytical and semi-preparative RP-HPLC was performed using a Shimadzu Prominence HPLC system with the column at room temperature (21–22 °C). Peptide mass was determined using matrix-assisted laser desorption/ionisation time-of-flight (MALDI-TOF) MS using a Model 4700 Proteomics Analyzer (Applied Biosystems, Foster City, CA, USA) collected in both positive reflector and linear mode. All masses reported are $M+H^+$. Fractions were mixed (1:1, v/v) with α-cyano-4-hydroxycinnamic acid matrix (7 mg/mL in 50% acetonitrile in H_2O). To obtain a sequence tag of the peptide the reductive matrix 1,5-diaminonaphthalene (1,5-DAN) was used (Fukuyama et al., 2006). The active fractions were mixed (1:1, v/v) with 1,5-DAN (10 mg/ml in 50% acetonitrile, 0.1% formic acid in H_2O).

2.3 Peptide sequencing.

The pure native peptide was reduced with 2-mercaptoethanol and alkylated by 4-vinyl-pyridinethen sequenced via N-terminal Edman degradation (477A, Applied Biosystems, Foster City, CA, USA). Sequence homologies were determined using sequences obtained from a search of non-redundant protein databases via the BLAST server. Sequence alignments and percentages of similarity were calculated using BLASTP (Altschul et al., 1997).

2.4 Production of recombinant Hm3a

Recombinant Hm3a was produced using the bacterial periplasmic expression system as described for PcTx1 (Klint et al., 2013; Saez et al., 2011). The synthetic gene encoding PcTx1_Δ3C was cloned into the pLicC-MBP expression vector, then mutated using standard PCR protocols to produce a vector encoding Hm3a (Qi and Scholthof, 2008). The fusion protein was expressed in *E.coli* BL21 (λDE3) and grown in Lysogeny broth medium to an OD_{600} of 0.8–1.0. The culture was then cooled to 16 °C and induced with 0.5 mM IPTG for 16 hours. Cells were pelleted by centrifugation at 5000 *g* then lysed via mechanical lysis at 28 kPa. The fusion protein was purified from the cell lysate via affinity chromatography using Ni-NTA Superflow resin (QIAGEN, Valencia, CA, USA). The peptide was cleaved from the fusion protein using TEV protease and purified by RP-HPLC on a C4 semi-preparative column (Phenomenex Jupiter, 250 x 10 mm, 300 Å). Peptide purity was verified using analytical RP-HPLC on a C18 column (Thermo Aquasil, 50 x 2.1 mm, 190 Å) and gradient of 10–50% solvent B over 40 min, at a flow rate of 0.25 ml/min. Masses of the eluted peptides were obtained using MALDI-TOF MS. The HPLC k' value [(peptide retention time – solvent retention time)/solvent retention time] for recombinant Hm3a was 23.5.

2.5 Electrophysiology

Peptide activity was assessed using two-electrode voltage-clamp (TEVC) electrophysiology on *Xenopus laevis* oocytes. Oocytes preparation, cDNA/cRNA preparation and injections were performed as described (Cristofori-Armstrong et al., 2015). Stage V–VI oocyte were injected with 20–40 ng of ion channel cDNA/cRNA (Nanoject 2000; WPI, Sarasota, FL, USA). Currents were recorded 1–6 days after injection under voltage-clamp using two standard glass microelectrodes of 0.5–2 MΩ resistance when filled with 3 M KCl solution. Oocytes were clamped at −60 mV (OC-725C oocyte clamp; Warner Instruments, Hamden, CT, USA). Currents were elicited by a drop in pH from 7.45 to 6.0 or 5.0 using a microperfusion system to allow rapid solution exchange (~1.5 ml/min) at room temperature. Conditioning pH of 7.45 was used for all experiments excluding mechanism of action studies at rASIC1a (activation and steady-state desensitization data), and rASIC1a_F350A mutant data performed using a conditioning pH of 7.35. HEPES was replaced by MES in buffers with pH below 6.8. A series of control currents were taken to account for the tachyphylaxis effect of ASICs in response to repeated pH stimulation prior to peptide application. Data were acquired (2000 Hz and filtered at 0.01 Hz) and analysis performed using pCLAMP software Version 10 (Axon Instruments, Sunnyvale, CA, USA). Peptides were prepared by serial dilutions in ND96 (96 mM NaCl, 1.8 mM $CaCl_2$, 2 mM KCl, 2 mM $MgCl_2$, 5 mM HEPES) solution supplemented with 0.1 % bovine serum albumin (BSA, fatty-acid free) to minimize adsorption to plastic surfaces.

2.6 Stability assays

Thermal stability was assessed by dissolving Hm3a, PcTx1 or oxytocin in 10 mM phosphate-buffered saline pH 7.4 to a final concentration of 25 μM. Samples were incubated at 55 °C and triplicate samples were taken at t = 0, 4, 8, 24, and 48, quenched with 5% TFA solution, centrifuged at 17 000 *g* for 25 minutes and analyzed using RP-HPLC. The peak

corresponding to intact peptide was identified by comparison to an untreated sample. Levels of peptide were quantified by integration of the peak area recorded at 214 nm, and plotted as a percentage of the peak area at $t = 0$ for each respective sample.

Serum stability was performed using male AB human serum (Sigma-Aldrich). Serum was pre-warmed to 37 °C for 15 minutes and added to lyophilized Hm3a, PcTx1, or oxytocin to a final concentration of 50 μM. Triplicate samples were taken at $t = 0$, 1, 2, 4, 8, 12, 24, and 48h for Hm3a and oxytocin, and $t = 0$, 2, 4, 24, and 48 h for PcTx1, quenched with 20% TFA solution, and stored at 4 °C for 15 minutes to precipitate serum proteins. Samples were centrifuged at 17 000 *g* for 25 minutes and analyzed using RP-HPLC. The peak corresponding to intact peptide was identified by comparison to an untreated sample and levels of peptide were quantified as described above.

2.7 Deposition of protein sequence information

Peptide sequence information derived for Hm3a has been submitted to the publicly accessible UniprotKB database (http://www.uniprot.org/) and has the accession number C0HKD0.

2.8 Materials

Chemicals were purchased from Sigma Aldrich (St. Louis, MO, USA, via Sigma Australia, Castle Hill, NSW, Australia), with the exceptions of isopropyl β-D-1-thiogalactopyranoside (IPTG) (Bioline, Alexandria, NSW, Australia) and TFA (Auspep Tullamarine, VIC, Australia). Recombinant TEV protease was produced in-house using a previously described protocol (Fang et al., 2007).

2.9 Animal welfare and ethics statement

Oocyte studies complied with the Australian code of practice for care and use of animals for scientific purposes, 8th Ed. 2013. The protocol was approved by The University of Queensland Animal Ethics Committee (Approval No. QBI/059/13/ARC/NHMRC). *Xenopus laevis* oocytes were obtained via recovery surgery performed under tricaine methanesulfonate anaesthesia (animals bathed in 1.3 mg/ml). All studies involving animals are reported in accordance with the ARRIVE guidelines for reporting experiments involving animals (Kilkenny et al., 2011; McGrath et al., 2010).

2.10 Data analysis and statistical procedures.

Data were analyzed with the software Graphpad Prism 6 (La Jolla, CA, USA). The half-maximal response (IC_{50}, EC_{50} or pH_{50}) and Hill coefficient (slope) were obtained through a non-linear fit to the data of a four parameter logistic equation ("sigmoidal dose-response"). Half-life ($t_{1/2}$) was obtained through a non-linear fit to the data of a "dissociation – one phase exponential decay" equation. Results are reported, in the text or on the figures, as means ± SEM. They represent the mean of *n* individual measurements on different oocytes. Statistical analysis and comparison between two groups was performed using Student's t-test with Welch's correction where standard deviations were not assumed to be equal. Comparisons of three or more groups were performed with one-way ANOVA and Tukey's Test for IC_{50} comparisons, and a two-way ANOVA and Tukey's Test for stability assays.

3. Results and Discussion

Despite sustained interest in ASIC1 as a promising drug target (Wemmie et al., 2013), the current array of ASIC1 modulatory ligands available as selective pharmacological tools and therapeutic leads is extremely limited. The difficulty in developing more selective small molecule ASIC inhibitors as therapeutic leads is illustrated by a series of medicinal chemistry studies by the Merck Research Laboratories. Three studies using different scaffolds all

resulted in more potent molecules against ASICs, however, all had significant off-target effects resulting in substantial sedation in animal studies (Kuduk et al., 2009a; Kuduk et al., 2010; Kuduk et al., 2009b). Based on the discovery of PcTx1 in a spider venom (Escoubas et al., 2000) as well as preliminary screening data from past studies (Escoubas, unpublished) we hypothesized that spider venoms, and especially tarantula venoms, should be a valuable source of additional novel ASIC modulators. Discovery of novel ligands, and understanding the molecular basis for differences in their biological properties (such as structural and chemical stability) and functions provides valuable insight to develop improved ligands.

3.1 Identification and purification of Hm3a

Screening a panel of spider venoms on rat ASIC1a expressed in *Xenopus laevis* oocytes revealed that *Heteroscodra maculata* (1/1000-fold dilution) venom robustly (>90%) inhibits this channel. Assay-guided fractionation led to the identification of a minor, early-eluting peptide (Fraction 12) responsible for the rASIC1a inhibitory activity (Figure 1A). The peptide has an observed monoisotopic $M+H^+$ of 4285.05 (Figure 1B) and was named π-TRTX-Hm3a, hereafter Hm3a, according to a rational nomenclature system for naming peptides from animal venoms (King et al., 2008).

The full-length amino acid sequence of Hm3a was determined using Edman degradation and verified using mass spectrometry. The theoretical oxidized monoisotopic m/z ($M+H^+$ = 4285.03) of the Hm3a sequence matched the observed monoisotopic mass, suggesting the presence of a free carboxylic acid at the C-terminus and three disulfide bonds. The Hm3a sequence matched that of another ASIC-inhibiting peptide previously isolated from this venom from an HPLC fraction of similar retention time and named Hm12 (Escoubas, unpublished).

Hm3a shares 82% identity with PcTx1, the prototypical ASIC1a inhibitor from *Psalmopoeus cambridgei* venom (Figure 1C). Hm3a differs from PcTx1 by five point mutations and a three-residue C-terminal truncation. Native Hm3a is highly potent on rASIC1a, inhibiting acid-evoked currents with an IC_{50} of 2.6 ± 1.3 nM when applied at pH 7.45 (Figure 1D and S1A). Due to the high sequence identity, conserved cysteine framework, and similar pharmacology between Hm3a and the inhibitor cysteine knot (ICK) fold peptide PcTx1 (PDB: 2KNI), it is highly likely that Hm3a also conforms to the ICK fold (Figure 1E).

3.2 Recombinant production of Hm3a

In order to obtain sufficient material to carry out further pharmacological characterization of Hm3a, we used an *Escherichia coli* recombinant expression system that we have previously employed to produce many disulfide rich venom peptides including PcTx1 (Klint et al., 2013; Saez et al., 2011). Following IPTG induction, the Hm3a-fusion protein was the dominant cellular protein present (Figure 2A) yielding ~1 mg of correctly folded peptide per liter of bacterial culture at >95% purity (determined using RP-HPLC and MS)(Figure 2B). The observed $M+H^+$ (4372.58) was in accordance with the calculated value (4372.06) for Hm3a with an additional N-terminal serine left over from the TEV recognition site (Figure 2B inset). The recombinant variant was subsequently used for all further characterization studies.

3.3 Effects of Hm3a on ASICs

Recombinant Hm3a was similarly potent to the native peptide with an IC_{50} of 1.3 ± 0.2 nM (Figure 3A) confirming that the determined sequence is responsible for the observed ASIC1a activity. Furthermore, it shows that the addition of an extra residue on the N-terminus (the serine from the TEV cleavage site) has little effect on the inhibitory activity of the peptide, consistent with the well-tolerated addition of a serine or tyrosine to the N-terminus of PcTx1 (Saez et al., 2011; Salinas et al., 2006). Having ascertained the functional integrity of the

recombinant Hm3a, the remaining characterization studies were performed using the recombinant peptide. The potency and selectivity of Hm3a was assessed using TEVC electrophysiology at a conditioning pH of 7.45 on oocytes expressing homomeric rASIC1a, rASIC1b, rASIC2a, rASIC3, human ASIC1a, hASIC1b, and co-expressed rASIC1a/ASIC1b (a potential mixture of homo- and heteromeric channels) (Figure 3A–B). Hm3a is highly selective for ASIC1, with no observable effect on rASIC2a or rASIC3 up to 10 μM (Figure 3A). In stark contrast, Hm3a strongly potentiated rASIC1b (~4-fold increase in current amplitude) with an EC_{50} of 46.5 ± 6.2 nM (Figure 3B), as has previously been reported for PcTx1 (Chen et al., 2006). The potentiating effect was also observed on heteromeric rASIC1a/ASIC1b channels with higher potency (EC_{50} of 17.4 ± 0.5 nM), but lower efficacy (less than 2-fold increase in current amplitude) as compared to homomeric rASIC1b (Figure 3B).

We next assessed species-dependent effects of Hm3a on ASIC1. Similar to the rat isoforms, Hm3a also inhibited hASIC1a (IC_{50} of 39.7 ± 1.1 nM) and potentiated hASIC1b (EC_{50} of 178.1 ± 1.3 nM); it was however ~30-fold, and ~3.8-fold less potent, respectively, than on the rat isoforms (Figure 3C). The Hill coefficients from the concentration-effect curves of Hm3a on both rat and human ASIC1a and ASIC1b were 1.3–1.6, suggesting positively cooperative binding of more than one Hm3a peptide per ASIC1 trimer. This is consistent with the co-crystal structures of cASIC1 and PcTx1 that showed up to three PcTx1 peptides bound per channel (see Figure 5A) (Baconguis and Gouaux, 2012; Dawson et al., 2012).

In the study by Chen *et al.* (Chen et al., 2006) that first demonstrated the potentiation of ASIC1b by PcTx1, the authors were unable to determine an accurate EC_{50} as a plateau in the PcTx1-induced potentiation effect was not reached. Here, we were able to show a maximal

response for Hm3a potentiation of both rat and human ASIC1b allowing more robust comparison of EC_{50} values. PcTx1 has been shown to inhibit both ASIC1a homomers (Escoubas et al., 2000) as well as rASIC1a/ASIC2b and rASIC1a/ASIC2a heteromers (Joeres et al., 2016; Sherwood et al., 2011), however, no activity has been reported on channels resulting from rASIC1a/ASIC1b co-expression (presumably containing heteromers). Our results indicate that rASIC1a/ASIC1b heteromers are sensitive to Hm3a in the mid-nanomolar range. A better understanding of the interaction of these peptides with both ASIC1b and ASIC1a/1b heteromers is crucial when they are used as ASIC1a inhibitors in animal studies because both ASIC1a and ASIC1b are highly expressed in the peripheral nervous system in rodents (Wu et al., 2004). The use of high concentrations of Hm3a or PcTx1 may lead to confounding results, and possible undesirable side-effects, because inhibition of ASIC1b has caused analgesic effects in inflammatory and nociceptive pain models in ASIC1a-knockout mice (Diochot et al., 2012).

Despite the high sequence identity of Hm3a to PcTx1, Hm3a is slightly less potent on rASIC1a (~3-fold compared to PcTx1 in our previous studies) (Saez et al., 2015; Saez et al., 2011) (Figure 1D and 3A). From our previous structure-activity studies on PcTx1, we have shown that truncation of the three C-terminal residues (Pro38, Lys39, Thr40; variant named Δ3C) resulted in a ~4-fold decrease in activity (Saez et al., 2015). Furthermore, a P38A mutation of PcTx1 was also ~4-fold less potent than wild-type PcTx1, leading us to the conclusion that the channel interaction mediated by Pro38 in PcTx1 could account for the slight loss in activity observed in Δ3C (Saez et al., 2015). Being equivalent in length to the PcTx1_Δ3C variant, Hm3a also lacks a proline at position 38. Hence, we hypothesized that the potency of Hm3a on rASIC1a could be enhanced by the addition of a proline at the C-terminus (Hm3a_P38). Hm3a_P38 had an IC_{50} of 0.4 ± 0.1 nM (Figure 3D) or a 3.3-fold

increase in potency as compared to wild-type recombinant Hm3a, in complete agreement with our prediction.

Extensive mutagenesis of PcTx1 (Saez et al., 2015; Saez et al., 2011), along with two co-crystal structures in complex with chicken ASIC1 (Baconguis and Gouaux, 2012; Dawson et al., 2012) have been instrumental in defining the PcTx1 pharmacophore. Three of the residue differences between PcTx1 and Hm3a (D2P, G9S, and E19A) were not identified as potential contacts in structural studies. As a result, the effect of these mutations in PcTx1 have not been studied, and here we show that these mutations do not appear to be crucial for activity against rASIC1a. Thr37 of PcTx1 was identified as a crystal contact, however a PcTx1_T37A mutant was shown to be equipotent with wild-type PcTx1 (Saez et al., 2015), in good agreement with the Hm3a potency at rASIC1a (Thr37 is a valine in Hm3a). The only residue difference between Hm3a and PcTx1 that falls within the key pharmacophore residues is R28K. Arg28 in PcTx1 makes multiple channel contacts and the PcTx1_R28A mutant had 14.5-fold lower activity on rASIC1a (Saez et al., 2015). In the case of Hm3a, the conservative mutation of arginine to lysine at position 28 appears to have little to no deleterious effect on peptide activity, thus the substitution is both functionally and structurally neutral. Although lysine has one less amino group, full retention of activity suggests that not all the interactions proposed in crystal studies are making energetically important contributions.

3.4 Mechanism of action of Hm3a on ASIC1

The homologous peptide PcTx1 mimics the binding of protons in the acidic pocket of ASIC1a, and inhibits channel currents by shifting the pH of half-maximal effect (pH_{50}) of steady-state desensitization (SSD) and activation to more alkaline values, pushing channels into a desensitized (non-conducting) state at pH 7.45 (Chen et al., 2005). Thus we assessed the effects of 30 nM Hm3a on SSD of rASIC1a (Figure 4A). Application of Hm3a in the

conditioning solution induced a parallel alkaline shift in the $pH_{50\ SSD}$ of rASIC1a by ~0.37 pH units from 7.24 ± 0.02 to 7.61 ± 0.02 (Figure 4C). This shift in SSD by Hm3a pushes ASIC1a into a desensitised state at pH 7.45 (i.e. inhibition), however at 30 nM the magnitude of the shift is insufficient to induce inhibition when applied at conditioning pH 7.9. Therefore at pH 7.9, the channels are in the resting state but in the presence of Hm3a. This allows us to study the effect of the peptide on the pH-dependence of channel activation, without the peptide inducing channel inhibition (Figure 4B). The pH_{50} of activation ($pH_{50\ ACT}$) of rASIC1a under control conditions was 6.08 ± 0.04, as compared to 6.28 ± 0.06 when conditioned with 30 nM Hm3a (Figure 4C). Thus Hm3a lowered the proton concentrations required for activation by ~0.20 pH units. The alkaline shift caused by Hm3a in the pH of both SSD and activation confirms the analogous mechanism of inhibition to PcTx1.

The on-rate of Hm3a on rASIC1a was examined by application of 30 nM peptide at pH 7.45 for increasing periods of time followed by activation at pH 6. Fitting a single exponential function to the time course of inhibition data revealed a time to 50% inhibition ($t_{1/2}$) of ~16 s, with maximal inhibition reached after ~90 s (Figure 4D). The slow onset of Hm3a inhibition may not be reflective of the actual binding on-rate for the peptide-channel interaction. Hm3a causes inhibition via inducing SSD of ASIC1a, which in itself is a slowly induced process (plateauing at >100 s for pH 7.05 exposure) (Babini et al., 2002), and likely takes longer than the actual on rate of Hm3a. In agreement with this, application of 30 nM Hm3a for less than 10 s led to potentiation of currents (Figure S3), indicative of a rapid interaction between ASIC1a and Hm3a, similar to previously reported observations with PcTx1 on rASIC1a (Chen et al., 2005). The on rate of Hm3a was similar to PcTx1 as previously reported using oocyte electrophysiology. Full inhibition of rASIC1a induced by 30 nM PcTx1 was achieved ~150 s after peptide application, with a time constant (Tau) of 52 s (Chen et al., 2006). Recovery of rASIC1a current after inhibition induced by a 180 s exposure to 30 nM Hm3a at

pH 7.45 was complete after ~360 s of peptide washout, with a $t_{1/2}$ of ~132 s (Figure 4E). ASIC1a recovers from the desensitized state over a time course of several seconds (time constant ~10 s) (Babini et al., 2002), hence the slower recovery from Hm3a inhibition can be largely attributed to unbinding of the peptide from the channel rather than simply recovery from SSD. Taken together, the mechanism and kinetics data shows that the homologous peptides Hm3a and PcTx1 have an almost identical effect on ASIC1a.

In order to determine the mechanism of ASIC1b potentiation by Hm3a, we analyzed the decay time constants of whole cell current desensitization. Control ASIC1b currents elicited by a pH drop to 5.0 decayed with a time constant (τ) of 1.28 ± 0.06 s (Figure 4F). Hm3a caused a concentration-dependent increase in the time constant of desensitization, and could be fit with the Hill function to yield an EC_{50} of 35.9 ± 17.2 nM, which is consistent with the EC_{50} determined for potentiation of peak current. Thus, Hm3a increases the time taken for channel desensitization, resulting in a prolonged open state that is observed as an increase in current amplitude consistent with the effect of PcTx1 on ASIC1b (Chen et al., 2006).

3.5 Characterizing the molecular interactions involved in subtype and species selectivity of Hm3a on ASIC1

The binding site of PcTx1 on ASIC1a was first studied using a chimeric channel approach (Chen et al., 2006; Salinas et al., 2006) and has since been extensively defined (Baconguis and Gouaux, 2012; Dawson et al., 2012; Saez et al., 2015; Saez et al., 2011). PcTx1 binds primarily to α-helix 5 at the bottom of the acidic pocket and a short stretch of residues following β-sheet 3 in the palm of the adjacent subunit (Figure 5A and 5B). The rASIC1a residue Phe350 (Phe352 in hASIC1a) on α-helix 5 in the thumb domain is particularly important for interaction with the peptide. Previous studies using diluted *Psalmopoeus cambridgei* venom (containing PcTx1) or recombinant PcTx1 on the hASIC1a_F352L or

rASIC1a_F350A mutants, respectively, showed a total lack of inhibition (Saez et al., 2015; Sherwood et al., 2009). However, shortly after, Sherwood *et al*., showed evidence that PcTx1 could still bind to the mutant channel (i.e., pre-incubation with 200 nM PcTx1 prevented the potentiating activity of big dynorphin) (Sherwood and Askwith, 2009). Given the similarity of Hm3a with PcTx1 in sequence and pharmacology we assume it will share the same binding site.

In order to confirm this, Hm3a was tested on the rASIC1a_F350A mutant. Our studies with higher concentrations (up to 10 μM) show that not only can Hm3a still bind, but also that it has an interesting dual functional effect (Figure 5C). Initial studies using a conditioning pH of 7.45 (to match that of all other concentration-effect data presented) showed that Hm3a strongly potentiated currents at concentrations over 300 nM. This effect was maximal at 3 μM (~2.8-fold increase in current amplitude), and a small decrease in the potentiation efficacy was seen at 10 μM. Given that Hm3a inhibits rASIC1a by inducing SSD and that the rASIC1a_F350A pH_{50} of SSD is shifted by ~0.1 units in the acidic direction compared to wild-type rASIC1a (Figure S4), the Hm3a concentration-effect curve was repeated using a conditioning pH of 7.35 (i.e., a conditioning pH that is ~0.2 pH units above the pH_{50} for SSD, thus equivalent to using pH 7.45 for wild-type rASIC1a). Under these conditions Hm3a, from 100 nM to 1 μM, once again potentiated currents (albeit with a much decreased efficacy), however at concentrations greater than 3 μM Hm3a induced channel inhibition. This suggests that despite losing the large number of contacts (five crystal contacts) made between Phe350 and PcTx1 (and by similarity, Hm3a) (Saez et al., 2015) there are still sufficient residual contacts to mediate a functional interaction at higher concentrations. It is thus tempting to speculate that during the potentiating effect (observed with lower peptide concentrations), Hm3a binds with partial occupancy and facilitates channel opening. Whereas, at higher concentrations the increased binding site occupancy (3 per channel) is sufficient to push

channels into the desensitised state. Another possible explanation could be that in the presence of the F350A mutation, Hm3a adopts a different orientation when bound, resulting in the complex concentration-dependent functional outcome observed in our study.

ASIC1b is highly expressed in peripheral sensory nerves and appears to play a key role in mediating acid-induced nociception, at least in rodents (Diochot et al., 2012; Hoagland et al., 2010). Thus determining the molecular basis for Hm3a potentiation of ASIC1b is an important step to understand potential complications when interpreting *in vivo* data, and enabling the design of more selective ASIC1 modulators. Thus, we further characterized the potential interactions sites of Hm3a on ASIC1. ASIC1a and ASIC1b are splice isoforms that only differ in the first third of the protein (identical from residue 186 of rASIC1a onwards). The use of a series of chimeras between rASIC1a and rASIC1b revealed a small stretch of residues 167–185 of rASIC1a (19 residues N-terminal to the splice-site) that are sufficient to confer the difference in peptide activity between rASIC1a and rASIC1b (inhibition vs potentiation)(coloured magenta in Figure 5B and sequence shown in Figure 5D) (Chen et al., 2006). Interestingly, the only residue difference within the known PcTx1 binding site between human and rat ASIC1a, is Ala178 in the rat channel (valine in hASIC1a) is also part of this small sequence stretch. We examined this region in further detail with rASIC1a point mutants for all PcTx1:cASIC1 crystal contact residues, predicting that several of the non-conserved residues should be responsible for the different subtype selectivity and species-specific pharmacology of Hm3a and PcTx1 at ASIC1 (Figure 5D and 5E).

The IC_{50} of Hm3a on rASIC1a_A178V (2.1 ± 0.7 nM) was only slightly increased compared to wild-type rASIC1a (Figure 5E), which does not account for the 30-fold difference in IC_{50} on rat and human ASIC1a. We concluded that Ala178 is not strongly involved in channel–peptide interaction, in agreement with molecular dynamics predictions

whereby the equivalent residue on cASIC1 (Gln179) does not form persistent interactions with PcTx1 (Saez et al., 2015). Furthermore, this finding is consistent with a previous study in which the mechanism of action of PcTx1 (*i.e.*, alkaline shift of SSD) was suggested to be responsible for the apparent lower potency of PcTx1 at hASIC1a compared to rodent ASIC1a, as the $pH_{50\ SSD}$ of hASIC1a is more acidic than that of the rat or mouse isoform (Sherwood and Askwith, 2008).

The IC_{50} of Hm3a on rASIC1a_H173S (1.8 ± 1.0 nM), rASIC1a_F174Y (1.9 ± 0.9 nM), and rASIC1a_A178P (2.1 ± 1.0 nM) was less than 2-fold different compared to that on wild-type rASIC1a. Consequently, these three residues are not likely to be making important interactions with the peptides for functional activity. In contrast, there was a significant decrease in Hm3a activity on both rASIC1a_R175C and rASIC1a_E177G, with an IC_{50} of 23.3 ± 1.1 nM and 13.2 ± 1.2 nM, respectively (Figure 5E). These mutations were made to make the rASIC1a-binding interface resemble that of rASIC1b. None of these mutations drastically affected the channels sensitivity to protons (in the form of pH-dependence of SSD and activation) (Figure S4), thus, any loss in potency is likely due to a loss of important interactions made between the peptide and channel, rather than changes in channel function or peptide mechanism. Consistent with this result, PcTx1:ASIC1 crystal structures and molecular dynamics studies (Baconguis and Gouaux, 2012; Dawson et al., 2012; Saez et al., 2015) showed that Arg175 and Glu177 of rASIC1a (Arg176 and Glu178 in cASIC1) make contact with Trp24 and Arg27 of PcTx1, respectively, both major pharmacophore residues (Saez et al., 2015; Saez et al., 2011). Although the interaction between PcTx1 and ASIC1a is well characterized, no study has so far demonstrated which individual residues determine subtype specificity between rASIC1a and rASIC1b. Here we show that Hm3a interacts with both ASIC1a and ASIC1b with a ~35-fold difference in potency (but different functional outcomes) and identified Arg175 and Glu177 of rASIC1a as two of the causative residues

which can account for the subtype specificity of Hm3a, and most likely PcTx1. This improved understanding of the binding interaction between peptide and channel should aid the design of more specific analogues of these peptides.

3.6 Stability of Hm3a and PcTx1

Given the likely role of ASIC1a in a range of pathological conditions, and the need to use selective pharmacological tools for target validation *in vivo*, it is important to understand the thermal and biological stability of peptides such as Hm3a and PcTx1. Despite its extensive use as a research tool *in vivo*, the stability of PcTx1 has never been reported. Therefore, we evaluated the stability of Hm3a and PcTx1 in comparison to the clinically used peptide oxytocin at 55 °C in phosphate-buffered saline at pH 7.4, and in human serum (Figure 6). Hm3a proved to have high thermal stability with ~10% loss after 48 h at 55 °C. In comparison, PcTx1 showed slightly more breakdown with ~24% loss after 48 h, and oxytocin showed a near-linear breakdown over time with ~38% of oxytocin remaining at 48 h. Similarly, Hm3a was largely unaffected in human serum with ~87% intact peptide after 48 h. In contrast, degradation of PcTx1 and oxytocin continued over the assay time with ~ 35% and ~40% of peptide respectively remaining after 48 h.

It is often claimed that ICK peptides are highly stable and resistant to thermal, chemical and enzymatic degradation and this has been demonstrated for several spider venom peptides, ω-Hv1a, ProTx-II, GsMTx-4, and GTx1-15 (Herzig and King, 2015; Kikuchi et al., 2015). Interestingly, despite their high degree of sequence similarity, Hm3a was more stable than PcTx1 when challenged with either high temperature or human serum. The improved stability of Hm3a over PcTx1 may be due to Hm3a's fewer charged residues (particularly lysines at the C-terminus), which are common cleavage sites for proteolytic enzymes such as trypsin (Olsen et al., 2004). We conclude that the substantially higher biological stability of Hm3a as

compared to PcTx1 makes it a substantially more attractive tool for studying the role of ASICs in biological fluids and in *in vivo* studies.

3.7 Off-target effects of Hm3a

Many spider venom peptides are gating modifiers of voltage-gated ion channels. Due to high suitability of Hm3a for *in vivo* studies, Hm3a was also tested on therapeutically-relevant off-targets including the rat voltage-gated sodium channel subtype 1.2 ($Na_V1.2$) and the voltage-gated potassium channel subtypes 10.1 ($K_V10.1$) and 11.1 ($K_V11.1$, or hERG). $Na_V1.2$ is predominantly expressed in the central nervous system and prolonged opening of the channel is implicated in the onset of epileptic disorders (Sugawara et al., 2001). $K_V10.1$ is implicated in a variety of cellular processes including cell proliferation and tumour progression (Ouadid-Ahidouch et al., 2016) whereas $K_V11.1$ is vital for cardiac function (Ouadid-Ahidouch et al., 2016). At 10 μM, Hm3a had no effect on the voltage-dependence of activation of these channels (Figure S5), suggesting a substantial selectivity of Hm3a towards ASIC1 over other ASICs subtypes as well as several voltage-gated channels.

5. Conclusions

We have identified and characterized a new potent peptide modulator of ASIC1 from the venom of *H. maculata*, and suspect that tarantula or other spider venoms may harbour even more, potent and selective peptide inhibitors of ASICs. Despite the high sequence and pharmacological similarity of Hm3a and PcTx1, Hm3a appears to be superior in terms of biological stability. Furthermore, through rational engineering of Hm3a, we produced a more potent variant of the peptide making its ASIC1a inhibitory potency on par with PcTx1. We also identified several determinant residues in rASIC1a for ASIC1a/1b selectivity studies. Overall, this study will contribute to the rational engineering and development of ASIC

modulators with improved subtype selectivity and facilitate the development of novel ASIC-targeting therapeutic leads and research tools.

Funding

We acknowledge financial support from the Australian National Health and Medical Research Council (NHMRC APP1067940; L.D.R.); S.Y.E. is supported by a UQ International Scholarship, and B. C-A. is supported by an Australian Postgraduate Award.

Conflict(s) of interest

None.

Acknowledgements

We thank Dr Jennifer Smith for helping with stability assays. We thank Prof. John Wood for the rat ASIC1a, ASIC2a, and ASIC3 clones; Prof. Stefan Gründer for the rat ASIC1b clone; A/Prof. Candice Askwith for the human ASIC1b clone; Prof. Richard Lewis for the rat $Na_V1.2$ clone; Dr Cas Simons for the $K_V10.1$ clone; and Prof. Jamie Vandenberg for the $K_V11.1$ clone.

Appendix A: Supplementary data

The following is supplementary data related to this article:

Supplemental Figure legends

Supplemental Figure 1. Example current traces from *Xenopus* oocyte data corresponding to concentration-response curves presented in Figures 1D and 3. (A) Native Hm3a isolated from venom inhibits rat ASIC1a (rASIC1a). Recombinant Hm3a activity at (B) rASIC1a, (C) rASIC2a, (D) rASIC3, (E) rASIC1b, (F) rASIC1a/1b heteromers (co-expression of RNAs in

oocyte), (G) human ASIC1a (hASIC1a), and (H) hASIC1b. (I) Recombinant Hm3a_P38 mutant activity at rASIC1a. Black boxes indicate peptide application with the corresponding concentration indicated above; grey boxes indicate pH stimulus; and the dashed line indicates current rundown that is independent of peptide application.

Supplemental Figure 2. Example current traces from *Xenopus* oocyte data corresponding to on- and off-rates presented in Figures 4D and E. (A and B) Representative traces of pH-evoked rASIC1a current inhibition by 30 nM Hm3a with varying degrees of application time as indicated by labels. (C) Example trace of rASIC1a recovery from inhibition with constant flow of peptide-free solution after 30 nM Hm3a application of 180 s. Currents were evoked every 60 s to assess recovery, and the dashed line indicates current rundown.

Supplemental Figure 3. Potentiation of rASIC1a currents by Hm3a with less than 10 s peptide exposure. (A) pH-stimulated currents are potentiated by application of Hm3a for 5 s, then from 10 s onwards, current inhibition increases with increased peptide exposure time as shown in Figure 4D (n = 4–7). (B) Representative traces of rASIC1a current potentiation by Hm3a application for 5s before pH stimulus with pH 5.0. Dashed line represents control current size and data for panel A are mean ± SEM.

Supplemental Figure 4. pH-dependence of (A) steady-state desensitization and (B) activation for wild-type and mutant rASIC1a channels used in this study (n = 6–8). (C) Half- maximal response (pH_{50}) and slope values for steady-state desensitization and activation curves from Hill function fits to the data (Prism 6). Data are mean ± SEM.

Supplemental Figure 5. The effect of 10 μM Hm3a on the voltage dependence of activation of the off-target channels (A) rat $Na_V1.2$, (B) human $K_V10.1$, and (C) human $K_V11.1$. Control curves are open circles and curves in the presence of Hm3a (10 μM) are filled circles with

solid line (n = 4–6). Data are mean ± SEM.

Supplemental Figure 6. Equivalent data set from Figure 5B showing the concentration-effect curves of Hm3a on the channel mutant rASIC1a_F350A, conditioned at both pH 7.45 (black) and pH 7.35 (red) (n = 6). Unlike Figure 5B, these data have been fit with the Hill function to obtain EC_{50} values. When calculating the regression for the pH 7.45 data, a range was set between 1 nM and 3 μM. Similarly, the data set collected at pH 7.35 has been fit with two equations with different ranges. The potentiation effect has been fit with the data between 1 nM and 1 μM, whereas the inhibition with data between 3 μM and 10 μM. Data are mean ± SEM.

References

Altschul, S. F., Madden, T. L., Schaffer, A. A., Zhang, J., Zhang, Z., Miller, W., Lipman, D. J., 1997. Gapped BLAST and PSI-BLAST: a new generation of protein database search programs. Nucleic Acids Res. 25, 3389–3402.

Babini, E., Paukert, M., Geisler, H. S., Grunder, S., 2002. Alternative splicing and interaction with di- and polyvalent cations control the dynamic range of acid-sensing ion channel 1 (ASIC1). J. Biol. Chem. 277, 41597–41603.

Baconguis, I., Gouaux, E., 2012. Structural plasticity and dynamic selectivity of acid-sensing ion channel-spider toxin complexes. Nature 489, 400–405.

Bagal, S. K., Brown, A. D., Cox, P. J., Omoto, K., Owen, R. M., Pryde, D. C., Sidders, B., Skerratt, S. E., Stevens, E. B., Storer, R. I., Swain, N. A., 2013. Ion channels as therapeutic targets: a drug discovery perspective. J. Med. Chem. 56, 593-624.

Baron, A., Lingueglia, E., 2015. Pharmacology of acid-sensing ion channels - Physiological and therapeutical perspectives. Neuropharmacol. 94, 19–35.

Bohlen, C. J., Chesler, A. T., Sharif-Naeini, R., Medzihradszky, K. F., Zhou, S., King, D., Sanchez, E. E., Burlingame, A. L., Basbaum, A. I., Julius, D., 2011. A heteromeric Texas coral snake toxin targets acid-sensing ion channels to produce pain. Nature 479, 410–414.

Boscardin, E., Alijevic, O., Hummler, E., Frateschi, S., Kellenberger, S., 2016. The function and regulation of acid-sensing ion channels (ASICs) and the epithelial Na(+) channel (ENaC): IUPHAR Review 19. Br. J. Pharmacol. 173, 2671-2701.

Chen, X., Kalbacher, H., Grunder, S., 2005. The tarantula toxin psalmotoxin 1 inhibits acid-sensing ion channel (ASIC) 1a by increasing its apparent H+ affinity. J. Gen. Physiol. 126, 71–79.

Chen, X., Kalbacher, H., Grunder, S., 2006. Interaction of acid-sensing ion channel (ASIC) 1 with the tarantula toxin psalmotoxin 1 is state dependent. J. Gen. Physiol. 127, 267–276.

Coryell, M. W., Wunsch, A. M., Haenfler, J. M., Allen, J. E., Schnizler, M., Ziemann, A. E., Cook, M. N., Dunning, J. P., Price, M. P., Rainier, J. D., Liu, Z., Light, A. R., Langbehn, D. R., Wemmie, J. A., 2009. Acid-sensing ion channel-1a in the amygdala, a novel therapeutic target in depression-related behavior. J. Neurosci. 29, 5381–5388.

Cristofori-Armstrong, B., Soh, M. S., Talwar, S., Brown, D. L., Griffin, J. D., Dekan, Z., Stow, J. L., King, G. F., Lynch, J. W., Rash, L. D., 2015. Xenopus borealis as an alternative source of oocytes for biophysical and pharmacological studies of neuronal ion channels. Sci Rep 5, 14763.

Dawson, R. J., Benz, J., Stohler, P., Tetaz, T., Joseph, C., Huber, S., Schmid, G., Hugin, D., Pflimlin, P., Trube, G., Rudolph, M. G., Hennig, M., Ruf, A., 2012. Structure of the acid-sensing ion channel 1 in complex with the gating modifier Psalmotoxin 1. Nat. Commun. 3, 936.

Deval, E., Noel, J., Lay, N., Alloui, A., Diochot, S., Friend, V., Jodar, M., Lazdunski, M., Lingueglia, E., 2008. ASIC3, a sensor of acidic and primary inflammatory pain. EMBO J. 27, 3047–3055.

Diochot, S., Baron, A., Salinas, M., Douguet, D., Scarzello, S., Dabert-Gay, A. S., Debayle, D., Friend, V., Alloui, A., Lazdunski, M., Lingueglia, E., 2012. Black mamba venom peptides target acid-sensing ion channels to abolish pain. Nature 490, 552–555.

Duan, B., Wu, L. J., Yu, Y. Q., Ding, Y., Jing, L., Xu, L., Chen, J., Xu, T. L., 2007. Upregulation of acid-sensing ion channel ASIC1a in spinal dorsal horn neurons contributes to inflammatory pain hypersensitivity. J. Neurosci. 27, 11139–11148.

Escoubas, P., De Weille, J. R., Lecoq, A., Diochot, S., Waldmann, R., Champigny, G., Moinier, D., Menez, A., Lazdunski, M., 2000. Isolation of a tarantula toxin specific for a class of proton-gated Na+ channels. J. Biol. Chem. 275, 25116–25121.

Fang, L., Jia, K. Z., Tang, Y. L., Ma, D. Y., Yu, M., Hua, Z. C., 2007. An improved strategy for high-level production of TEV protease in Escherichia coli and its purification and characterization. Protein Expr. Purif. 51, 102–109.

Fukuyama, Y., Iwamoto, S., Tanaka, K., 2006. Rapid sequencing and disulfide mapping of peptides containing disulfide bonds by using 1,5-diaminonaphthalene as a reductive matrix. J. Mass Spectrom. 41, 191–201.

Herzig, V., King, G. F., 2015. The Cystine Knot Is Responsible for the Exceptional Stability of the Insecticidal Spider Toxin omega-Hexatoxin-Hv1a. Toxins (Basel) 7, 4366–4380.

Hesselager, M., Timmermann, D. B., Ahring, P. K., 2004. pH Dependency and desensitization kinetics of heterologously expressed combinations of acid-sensing ion channel subunits. J. Biol. Chem. 279, 11006–11015.

Hoagland, E. N., Sherwood, T. W., Lee, K. G., Walker, C. J., Askwith, C. C., 2010. Identification of a calcium permeable human acid-sensing ion channel 1 transcript variant. J. Biol. Chem. 285, 41852–41862.

Jasti, J., Furukawa, H., Gonzales, E. B., Gouaux, E., 2007. Structure of acid-sensing ion channel 1 at 1.9 Å resolution and low pH. Nature 449, 316–323.

Joeres, N., Augustinowski, K., Neuhof, A., Assmann, M., Grunder, S., 2016. Functional and pharmacological characterization of two different ASIC1a/2a heteromers reveals their sensitivity to the spider toxin PcTx1. Sci. Rep. 6, 27647.

Kikuchi, K., Sugiura, M., Kimura, T., 2015. High Proteolytic Resistance of Spider-Derived Inhibitor Cystine Knots. Int. J. Pept. 2015, 537508.

Kilkenny, C., Browne, W., Cuthill, I. C., Emerson, M., Altman, D. G., National Centre for the Replacement, R., Reduction of Amimals in, R., 2011. Animal research: reporting in vivo experiments--the ARRIVE guidelines. J. Cereb. Blood Flow Metab. 31, 991–993.

King, G. F., Gentz, M. C., Escoubas, P., Nicholson, G. M., 2008. A rational nomenclature for naming peptide toxins from spiders and other venomous animals. Toxicon 52, 264–276.

Klint, J. K., Senff, S., Rupasinghe, D. B., Er, S. Y., Herzig, V., Nicholson, G. M., King, G. F., 2012. Spider-venom peptides that target voltage-gated sodium channels: pharmacological tools and potential therapeutic leads. Toxicon 60, 478–491.

Klint, J. K., Senff, S., Saez, N. J., Seshadri, R., Lau, H. Y., Bende, N. S., Undheim, E. A., Rash, L. D., Mobli, M., King, G. F., 2013. Production of recombinant disulfide-rich venom peptides for structural and functional analysis via expression in the periplasm of E. coli. PLoS One 8, e63865.

Kuduk, S. D., Chang, R. K., Wai, J. M., Di Marco, C. N., Cofre, V., DiPardo, R. M., Cook, S. P., Cato, M. J., Jovanovska, A., Urban, M. O., Leitl, M., Spencer, R. H., Kane, S. A., Hartman, G. D., Bilodeau, M. T., 2009a. Amidine derived inhibitors of acid-sensing ion channel-3 (ASIC3). Bioorg. Med. Chem. Lett. 19, 4059–4063.

Kuduk, S. D., Di Marco, C. N., Bodmer-Narkevitch, V., Cook, S. P., Cato, M. J., Jovanovska, A., Urban, M. O., Leitl, M., Sain, N., Liang, A., Spencer, R. H., Kane, S. A., Hartman, G. D., Bilodeau, M. T., 2010. Synthesis, structure-activity relationship, and pharmacological profile of analogs of the ASIC-3 inhibitor A-317567. ACS Chem. Neurosci. 1, 19–24.

Kuduk, S. D., Di Marco, C. N., Chang, R. K., Dipardo, R. M., Cook, S. P., Cato, M. J., Jovanovska, A., Urban, M. O., Leitl, M., Spencer, R. H., Kane, S. A., Bilodeau, M. T., Hartman, G. D., Bock, M. G., 2009b. Amiloride derived inhibitors of acid-sensing ion channel-3 (ASIC3). Bioorg. Med. Chem. Lett. 19, 2514–2518.

McCarthy, C. A., Rash, L. D., Chassagnon, I. R., King, G. F., Widdop, R. E., 2015. PcTx1 affords neuroprotection in a conscious model of stroke in hypertensive rats via selective inhibition of ASIC1a. Neuropharmacol. 99, 650–657.

McGrath, J. C., Drummond, G. B., McLachlan, E. M., Kilkenny, C., Wainwright, C. L., 2010. Guidelines for reporting experiments involving animals: the ARRIVE guidelines. Br. J. Pharmacol. 160, 1573–1576.

Nebe, J., Ebersberger, A., Vanegas, H., Schaible, H. G., 1999. Effects of omega-agatoxin IVA, a P-type calcium channel antagonist, on the development of spinal neuronal hyperexcitability caused by knee inflammation in rats. J. Neurophysiol. 81, 2620–2626.

Olsen, J. V., Ong, S. E., Mann, M., 2004. Trypsin cleaves exclusively C-terminal to arginine and lysine residues. Mol. Cell. Proteomics 3, 608–614.

Osteen, J. D., Herzig, V., Gilchrist, J., Emrick, J. J., Zhang, C., Wang, X., Castro, J., Garcia-Caraballo, S., Grundy, L., Rychkov, G. Y., Weyer, A. D., Dekan, Z., Undheim, E. A., Alewood, P., Stucky, C. L., Brierley, S. M., Basbaum, A. I., Bosmans, F., King, G. F., Julius, D., 2016. Selective spider toxins reveal a role for the Nav1.1 channel in mechanical pain. Nature 534, 494–499.

Ouadid-Ahidouch, H., Ahidouch, A., Pardo, L. A., 2016. $K_V10.1$ K(+) channel: from physiology to cancer. Pflugers Arch. 468, 751–762.

Qi, D., Scholthof, K. B., 2008. A one-step PCR-based method for rapid and efficient site-directed fragment deletion, insertion, and substitution mutagenesis. J. Virol. Methods 149, 85–90.

Saez, N. J., Deplazes, E., Cristofori-Armstrong, B., Chassagnon, I. R., Lin, X., Mobli, M., Mark, A. E., Rash, L. D., King, G. F., 2015. Molecular dynamics and functional studies define a hot spot of crystal contacts essential for PcTx1 inhibition of acid-sensing ion channel 1a. Br. J. Pharmacol. 172, 4985–4995.

Saez, N. J., Mobli, M., Bieri, M., Chassagnon, I. R., Malde, A. K., Gamsjaeger, R., Mark, A. E., Gooley, P. R., Rash, L. D., King, G. F., 2011. A dynamic pharmacophore drives the interaction between Psalmotoxin-1 and the putative drug target acid-sensing ion channel 1a. Mol. Pharmacol. 80, 796–808.

Saez, N. J., Senff, S., Jensen, J. E., Er, S. Y., Herzig, V., Rash, L. D., King, G. F., 2010. Spider-venom peptides as therapeutics. Toxins (Basel) 2, 2851–2871.

Salinas, M., Rash, L. D., Baron, A., Lambeau, G., Escoubas, P., Lazdunski, M., 2006. The receptor site of the spider toxin PcTx1 on the proton-gated cation channel ASIC1a. J. Physiol. 570, 339–354.

Sherwood, T., Franke, R., Conneely, S., Joyner, J., Arumugan, P., Askwith, C., 2009. Identification of protein domains that control proton and calcium sensitivity of ASIC1a. J. Biol. Chem. 284, 27899–27907.

Sherwood, T. W., Askwith, C. C., 2008. Endogenous arginine-phenylalanine-amide-related peptides alter steady-state desensitization of ASIC1a. J. Biol. Chem. 283, 1818-1830.

Sherwood, T. W., Askwith, C. C., 2009. Dynorphin opioid peptides enhance acid-sensing ion channel 1a activity and acidosis-induced neuronal death. J. Neurosci. 29, 14371–14380.

Sherwood, T. W., Lee, K. G., Gormley, M. G., Askwith, C. C., 2011. Heteromeric acid-sensing ion channels (ASICs) composed of ASIC2b and ASIC1a display novel channel properties and contribute to acidosis-induced neuronal death. J. Neurosci. 31, 9723–9734.

Siemens, J., Zhou, S., Piskorowski, R., Nikai, T., Lumpkin, E. A., Basbaum, A. I., King, D., Julius, D., 2006. Spider toxins activate the capsaicin receptor to produce inflammatory pain. Nature 444, 208–212.

Sugawara, T., Tsurubuchi, Y., Agarwala, K. L., Ito, M., Fukuma, G., Mazaki-Miyazaki, E., Nagafuji, H., Noda, M., Imoto, K., Wada, K., Mitsudome, A., Kaneko, S., Montal, M.,

Nagata, K., Hirose, S., Yamakawa, K., 2001. A missense mutation of the Na^+ channel alpha II subunit gene Na(v)1.2 in a patient with febrile and afebrile seizures causes channel dysfunction. Proc. Natl. Acad. Sc.i USA 98, 6384–6389.

Vergo, S., Craner, M. J., Etzensperger, R., Attfield, K., Friese, M. A., Newcombe, J., Esiri, M., Fugger, L., 2011. Acid-sensing ion channel 1 is involved in both axonal injury and demyelination in multiple sclerosis and its animal model. Brain 134, 571–584.

Waldmann, R., Champigny, G., Bassilana, F., Heurteaux, C., Lazdunski, M., 1997. A proton-gated cation channel involved in acid-sensing. Nature 386, 173–177.

Wemmie, J. A., Taugher, R. J., Kreple, C. J., 2013. Acid-sensing ion channels in pain and disease. Nat. Rev. Neurosci. 14, 461–471.

Wu, L. J., Duan, B., Mei, Y. D., Gao, J., Chen, J. G., Zhuo, M., Xu, L., Wu, M., Xu, T. L., 2004. Characterization of acid-sensing ion channels in dorsal horn neurons of rat spinal cord. J. Biol. Chem. 279, 43716–43724.

Xiong, Z. G., Zhu, X. M., Chu, X. P., Minami, M., Hey, J., Wei, W. L., MacDonald, J. F., Wemmie, J. A., Price, M. P., Welsh, M. J., Simon, R. P., 2004. Neuroprotection in ischemia: blocking calcium-permeable acid-sensing ion channels. Cell 118, 687–698.

Yermolaieva, O., Leonard, A. S., Schnizler, M. K., Abboud, F. M., Welsh, M. J., 2004. Extracellular acidosis increases neuronal cell calcium by activating acid-sensing ion channel 1a. Proc. Natl. Acad. Sci. USA 101, 6752–6757.

Ziemann, A. E., Schnizler, M. K., Albert, G. W., Severson, M. A., Howard, M. A., 3rd, Welsh, M. J., Wemmie, J. A., 2008. Seizure termination by acidosis depends on ASIC1a. Nat. Neurosci. 11, 816–822.

Figure Legends

Figure 1. Isolation of Hm3a from *H. maculata* venom. (A) RP-HPLC chromatogram of crude *H. maculata* venom indicating the Hm3a containing Frac 12*. Inset: effect of Frac 12* on rASIC1a. (B) Chromatogram showing the final purification step of native Hm3a and MALDI-TOF mass spectrum showing a monoisotopic $M+H^+$ of 4285.05. (C) Amino acid sequence of Hm3a aligned with PcTx1 (grey background = conserved residues, red = cysteine residues and disulfide connectivity shown below). (D) Concentration-effect curve for inhibition of rASIC1a by native Hm3a conditioned at pH 7.45 yielded an IC_{50} of 2.6 ± 1.3 nM (n = 6; error bars denote SEM). (E) Homology model of Hm3a (based on PcTx1 NMR structure, PDB: 2KNI) in blue. PcTx1 NMR structure in green, with the disulfide bridges in both shown in red, and N- and C-termini are as indicated.

Figure 2. Production of recombinant Hm3a (A) SDS-PAGE gel showing the expression, purification and TEV cleavage of the Hm3a-MBP fusion protein. Lanes are as follows: MW marker; Uninduced and Induced (IPTG) whole-cell extract; Insoluble and soluble fraction after cell lysis; Flow-through, soluble cell lysate after passed through Ni-NTA; Wash, eluate from 15 mM imidazole wash; Elution, fusion protein eluted by 250 mM imidazole; Concentrated fusion protein before and after cleavage with TEV protease. (B) RP-HPLC chromatogram of purified recombinant Hm3a. Inset is a MALDI-TOF mass spectrum showing the monoisotopic $M+H^+$ of 4372.58 (calculated 4372.06). Recombinant Hm3a contains a vestigial N-terminal serine from the TEV cleavage.

Figure 3. Concentration-effect curves of recombinant Hm3a for (A) homomeric rASIC1a, rASIC2a, and rASIC3 (n = 6–10), (B) homomeric rASIC1b and heteromeric rASIC1a/ASIC1b channels (heteromeric rASIC1a/ASIC1b is the response observed in oocytes co-injected with both rASIC1a and rASIC1b cRNA) (n = 6), and (C) homomeric hASIC1a and hASIC1b (n = 7). (D) Concentration-effect curves of Hm3a_WT and Hm3a_P38 mutant on homomeric rASIC1a (n = 4–10). *Statistical comparison of $logEC_{50}$ between rASIC1b and heteromeric rASIC1a/ASIC1b data sets (panel B); p = 0.0052 and F = 8.069, and $logIC_{50}$ for Hm3a WT and P38 mutant data sets (panel D); p = 0.0029 and F = 9.388. Conditioning pH used to generate all the above data was pH 7.45, and example traces are shown in Supplementary Figure 1. Data are mean ± SEM.

Figure 4. Mechanism of action of Hm3a on rASIC1. (A) Representative steady-state desensitization (SSD) current traces in the absence (top) or presence (bottom) of 30 nM Hm3a, currents elicited by pH 6.0 following conditioning (cond.) from pH 7.9 to 7.1. (B) Representative pH-activation current traces in absence (top) or presence (bottom) of 30 nM Hm3a, elicited by pH 5.0 to 7.0. (C) SSD and activation curves of rASIC1a in the absence and presence of 30 nM Hm3a (n = 6). Statistical comparison of pH_{50} between control and Hm3a data sets; SSD, $p < 0.0001$ and $F = 379.1$; Activation, $p = 0.0219$ and $F = 5.526$. (D) Time course of rASIC1a inhibition by 30 nM Hm3a. The $t_{1/2}$ was calculated from a single-exponential decay function (n = 6). (E) Recovery of rASIC1a from inhibition by 30 nM Hm3a. The $t_{1/2}$ was calculated a single-exponential function fit to the data (n = 6). Representative current traces for panels D and E are shown in Supplementary Figure 2. (F) Time constants (τ) of rASIC1b desensitization for control conditions and with increasing concentrations of Hm3a. Dashed line represents a fit of the Hill equation (n = 5). Inset: effect of 1 μM Hm3a on rASIC1b with Hm3a potentiated current (dotted line) normalized to control (solid line) peak height to better visualize slowed channel desensitization by Hm3a. Data are mean ± SEM.

Figure 5. Molecular interactions involved in species and subtype selectivity. (A) Structure of the PcTx1:cASIC1 complex (PDB: 3S3X) viewed from above. The three cASIC1 subunits are colored green, orange, and blue, and the three PcTx1 molecules (grey) are shown bound at the subunit interfaces. (B) Molecular surfaces of the complex indicating the 19-residue region (amino acids 167–185, highlighted in magenta) that determines functional inhibition of rASIC1a by PcTx1[34]. (C) Concentration-effect curves of Hm3a on rASIC1a_F350A when conditioning the channel at both pH 7.45 (black circles) and pH 7.35 (red squares) (n = 6) (illustrated using a lowness fit, see Figure S4 for fits with the Hill function for potency determination). (D) Sequence alignment of ASIC subtypes showing the 19 residue functionally important region for PcTx1 (and by similarity Hm3a)(colored magenta in panel B). Cyan = residues identical in all subtypes, grey = semi-conserved residues (i.e. identical to rASIC1a). Channel residues in rASIC1a that correspond to cASIC1 crystal contacts were mutated in this study, and the residue they were mutated to are bolded. (E) Concentration-effect curves for Hm3a at wild-type rASIC1a and point mutants (n = 6–10). A statistically significant difference from rASIC1a WT in $logIC_{50}$ inhibition by Hm3a was present for both rASIC1a R175C and E177G mutants, $p < 0.0001$, represented by *. Data for panel E were performed using a conditioning pH of 7.45. Data are mean ± SEM.

Figure 6. Comparative stability studies of Hm3a and PcTx1. (A) Thermal stability of Hm3a, PcTx1 and oxytocin at 55 °C (pH 7.4, phosphate-buffered saline). (B) Serum stability of Hm3a, PcTx1 and oxytocin at 37 °C. The percentage of peptide remaining for all conditions was quantified using RP-HPLC (n = 3–5). (C) Example RP-HPLC profile at 214 nm of Hm3a and PcTx1 following incubation in human serum at 0 h (black), 24 h (blue) and 48 h (red). Data are mean ± SEM, and statistical analyses are comparisons between Hm3a and PcTx1 at a given time point (* represents $p > 0.05$, and ns is not significant).

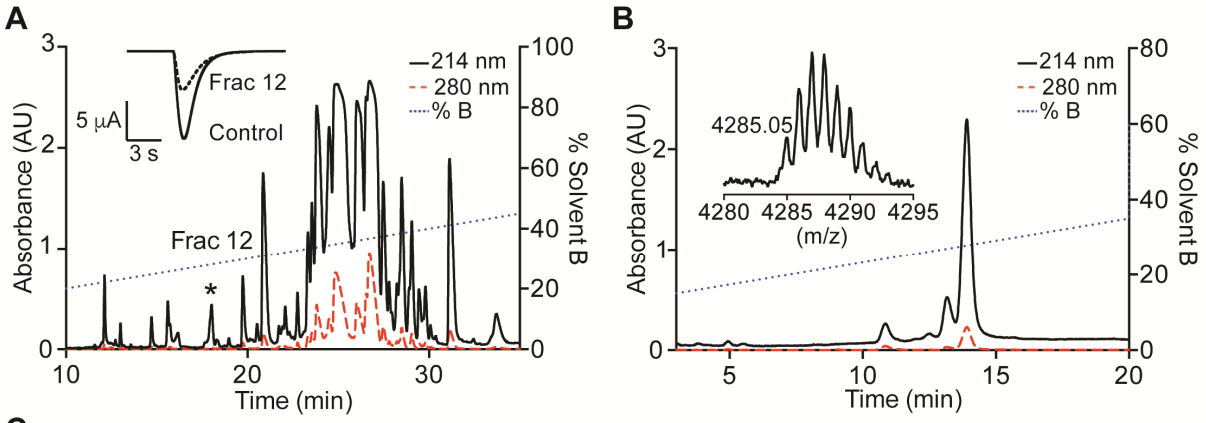

C

Peptide	Sequence	Theoretical (M+H⁺)	% Identity
Hm3a	EPCIPKWKSCVNRHGDCCAGLECWKRRKSFEVCVPKV---	4285.03	82%
PcTx1	EDCIPKWKGCVNRHGDCCEGLECWKRRRSFEVCVPKTPKT	4686.17	

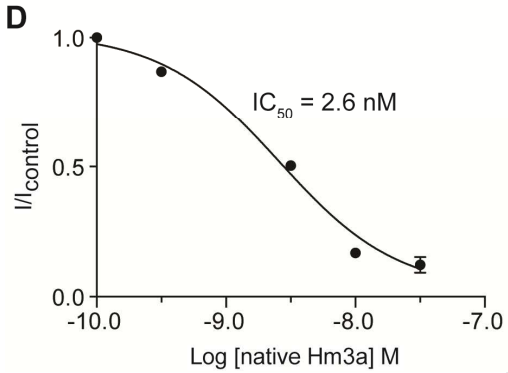

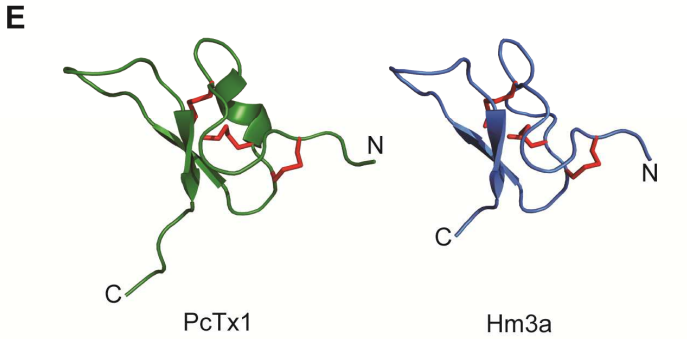

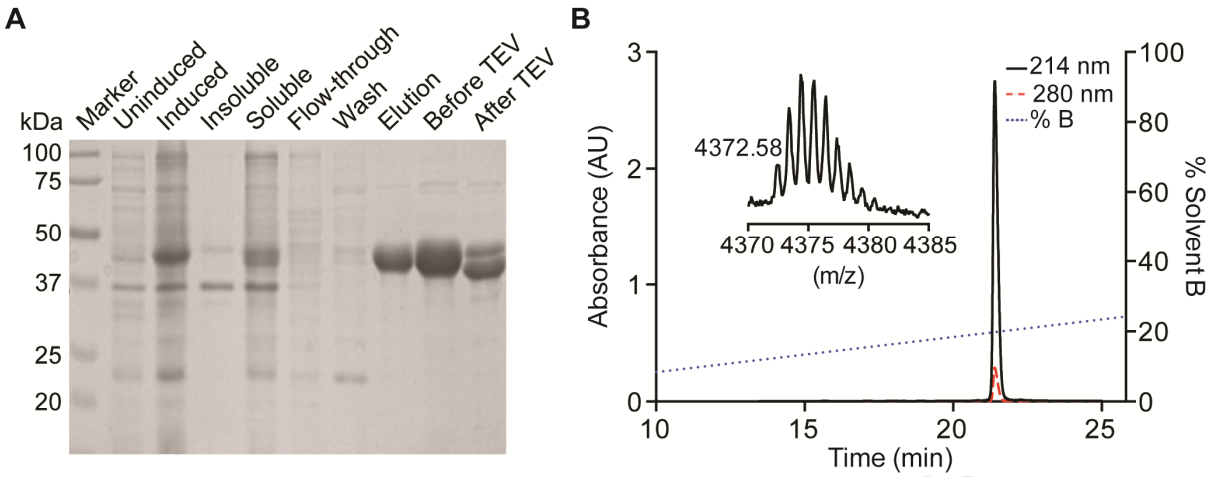

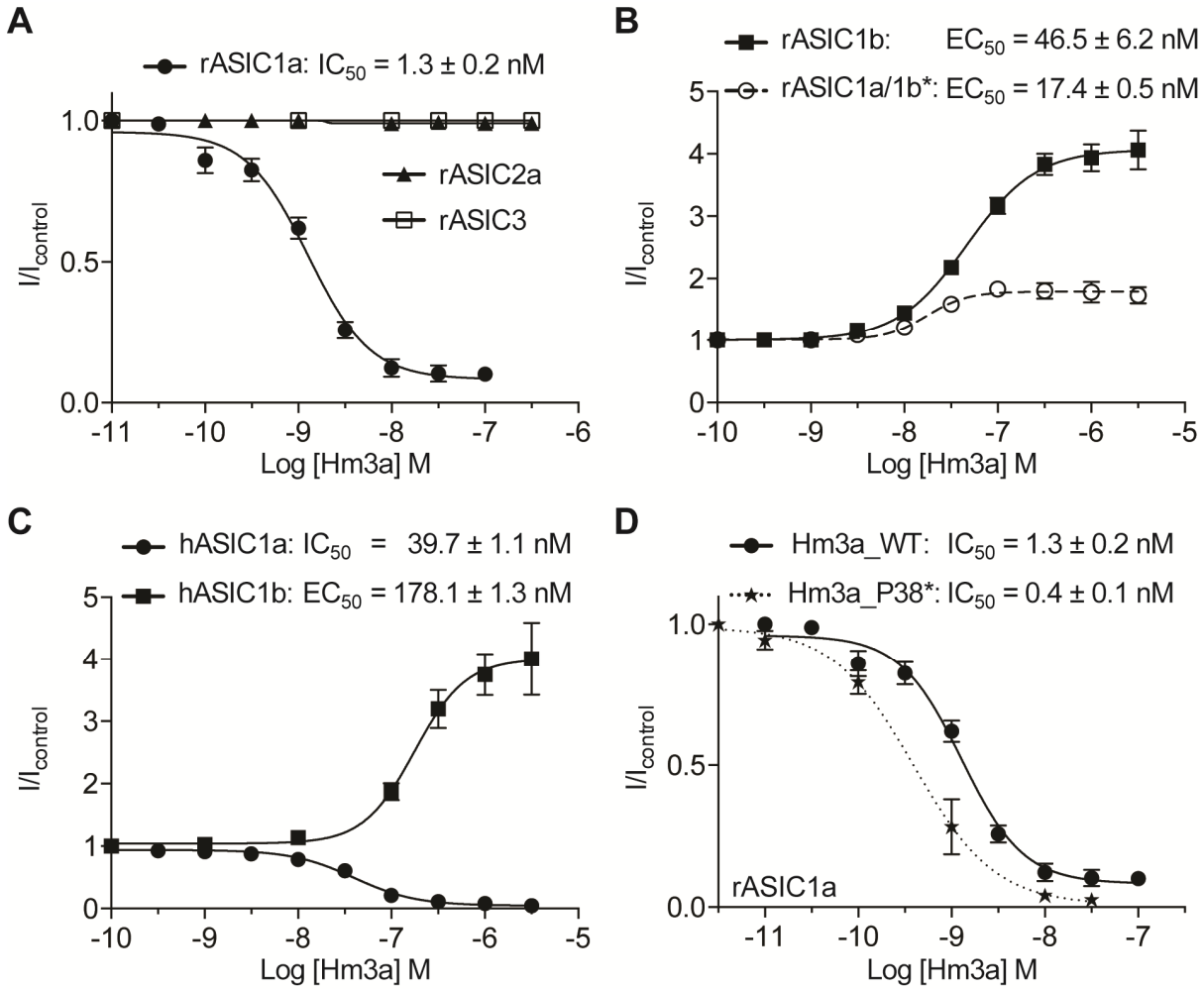
A
rASIC1a: IC50 = 1.3 ± 0.2 nM
rASIC2a
rASIC3
I/Icontrol
Log [Hm3a] M
B
rASIC1b: EC50 = 46.5 ± 6.2 nM
rASIC1a/1b*: EC50 = 17.4 ± 0.5 nM
I/Icontrol
Log [Hm3a] M
C
hASIC1a: IC50 = 39.7 ± 1.1 nM
hASIC1b: EC50 = 178.1 ± 1.3 nM
I/Icontrol
Log [Hm3a] M
D
Hm3a_WT: IC50 = 1.3 ± 0.2 nM
Hm3a_P38*: IC50 = 0.4 ± 0.1 nM
rASIC1a
I/Icontrol
Log [Hm3a] M

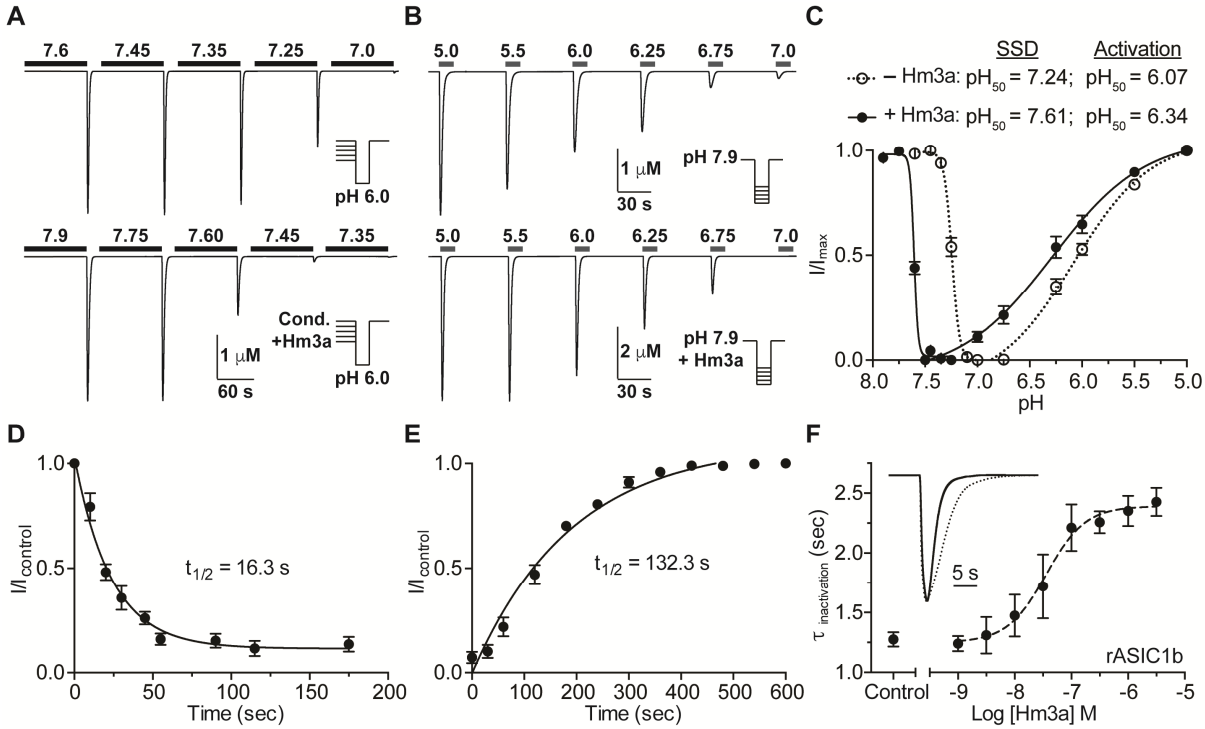

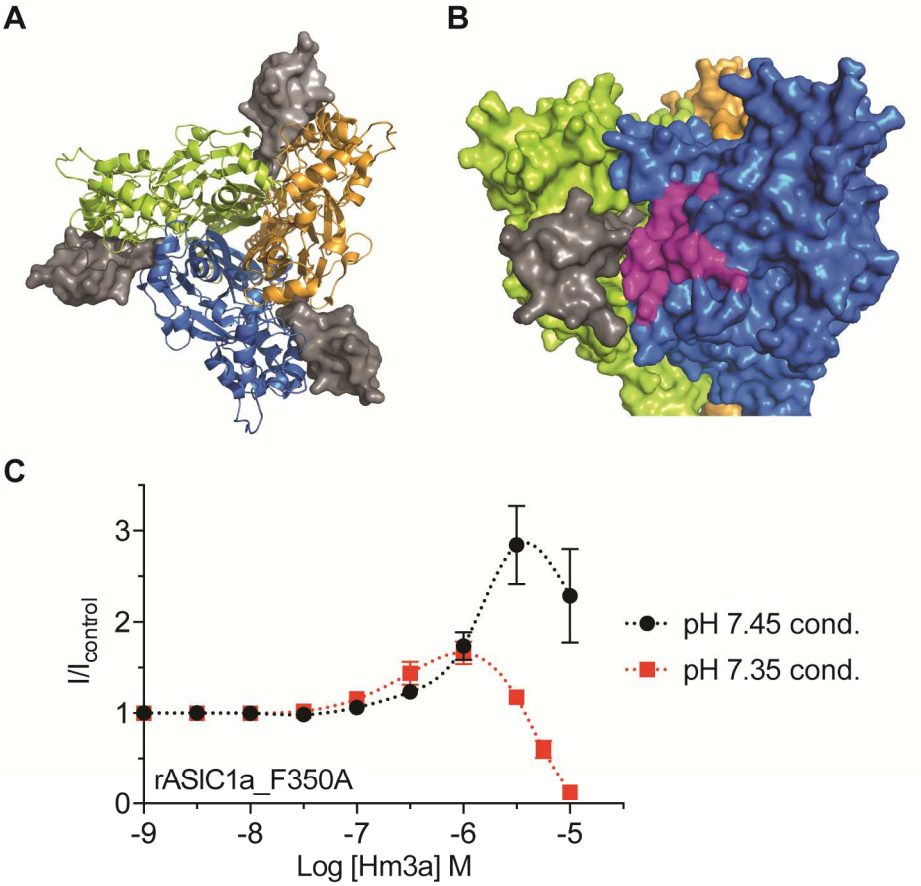

D

cASIC1	168	EMLLSCFFRGEQCSPEDFK	186
rASIC1a	167	DMLLSC**HFR**G**EA**CSAEDFK	185
hASIC1a	167	DMLLSCHFRGE**V**CSAEDFK	185
rASIC1b	194	DMLLYC**SYC**G**GP**CGPHNFS	218

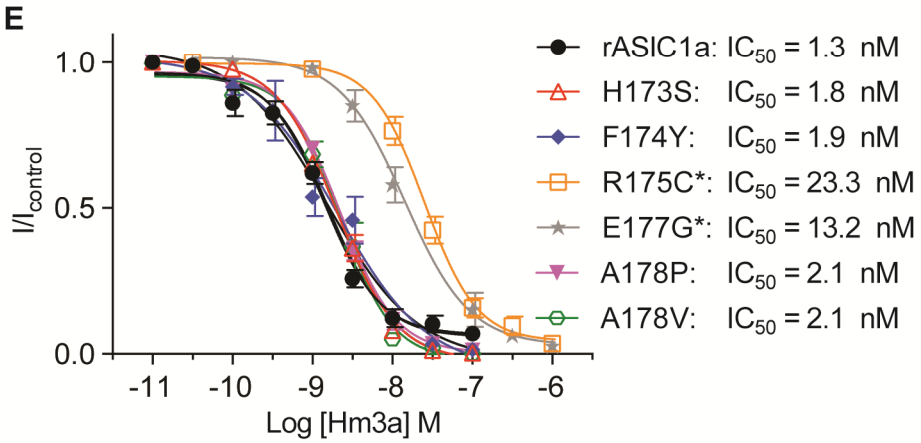

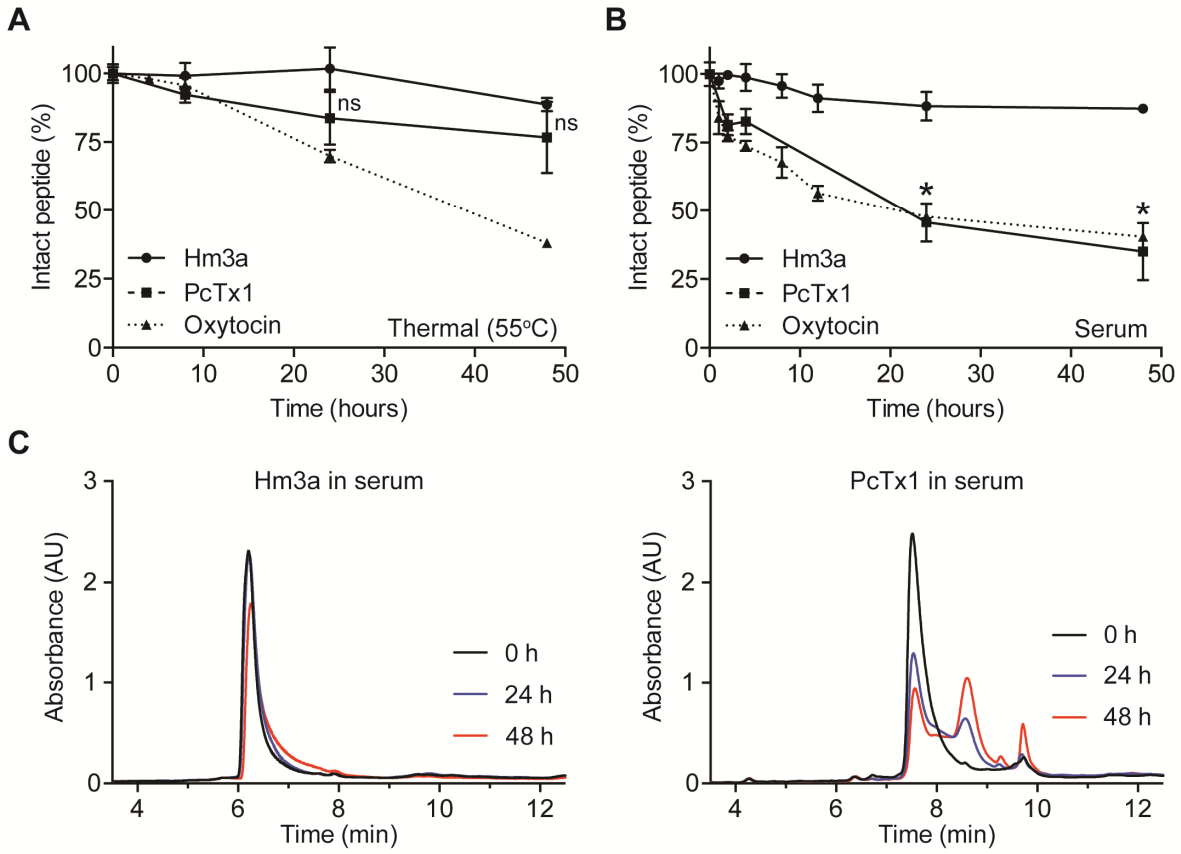

Discovery and molecular interaction studies of a highly stable, tarantula peptide modulator of acid-sensing ion channel 1

Highlights:

- Hm3a is an ASIC1 modulating peptide isolated from Togo starburst tarantula venom.
- Hm3a is a truncated variant of PcTx1 with very similar pharmacological activity.
- ASIC1a residues E177 and R175 are important for subtype-dependent effects of Hm3a.
- Hm3a is substantially more biologically stable than PcTx1 over 48 hours.

Highlights

Highlights are mandatory for this journal. They consist of a short collection of bullet points that convey the core findings of the article and should be submitted in a separate editable file in the online submission system. Please use 'Highlights' in the file name and include 3 to 5 bullet points (maximum 85 characters, including spaces, per bullet point). You can view example Highlights on our information site.